Available online at www.sciencedirect.com

ScienceDirect

journal homepage: www.intl.elsevierhealth.com/journals/dema

Effect of loading configuration on strength values in a highly transformable zirconia-based composite

Imane Touaiher[a,*], *Malika Saâdaoui*[a], *Jérôme Chevalier*[b], *Helen Reveron*[b]

[a] *Université Mohamed V, EMI, LERSIM, Avenue Ibn Sina, B.P. 765, Rabat, Morocco*
[b] *Université de Lyon, INSA de Lyon, MATEIS CNRS UMR5510, 20 Avenue Albert Einstein, F-69621 Villeurbanne Cedex, France*

ARTICLE INFO

Article history:
Received 7 March 2016
Received in revised form
17 May 2016
Accepted 29 June 2016

Keywords:
Zirconia composite
Autocatalytic transformation
Strength
Piston-on-three balls test

ABSTRACT

Objectives. The aim of this work was to determine mechanical properties of a highly transformable 10Ce-TZP/Al_2O_3/La_2AlO_3 composite, currently developed as a biomaterial for dental application, and to investigate the effect of loading configuration on its flexural strength.

Methods. Fracture toughness is determined by the single-edge-V-notched beam (SEVNB) method. Strength measurements were conducted by four-point bending and biaxial bending tests (piston-on-three balls) according to ISO 6872, dedicated to ceramic materials in dentistry.

Results. Strength obtained by either four-point or biaxial bending are very different, and take the values of 596 MPa and 1470 MPa respectively. It is demonstrated that the difference in measured strength cannot be attributed to the effect of volume on strength, generally predicted by the standard Weibull analysis, but to different transformation behaviors for the two bending configurations. More extensive transformation occurs in the biaxial configuration, with a lower autocatalytic transformation stress threshold, resulting to substantial compressive residual stresses.

Significance. The significant influence of the loading configuration on the strength should be integrated when designing a component from a highly transformable ceramic.

1. Introduction

Zirconia toughened ceramics (ZTC) are attractive materials for several medical and engineering applications as they exhibit high strength and toughness compared to other oxide ceramics. These superior properties result from the stress induced tetragonal to monoclinic phase transformation occurring in these materials. During crack propagation, the volume increase (~4%) accompanying the transformation creates compressive stresses that shield the crack tip from the applied stress and thus, enhances the fracture toughness [1–4]. The properties of ZTC depend on their microstructure and composition, especially the amount of transformable tetragonal phase. The major difficulty for the development of transformation-toughened zirconia composites is to combine high strength and high toughness, as the strength is limited by the stress-activated transformation in these materials [4,5]. For example, ceria-doped zirconia (Ce-TZP) can exhibit high toughness (more than 15 MPa $m^{1/2}$) but moderate

* *Corresponding author*. Tel.: +212 669366403.
E-mail address: imanetouaiher@gmail.com (I. Touaiher).
http://dx.doi.org/10.1016/j.dental.2016.06.023

strength (300–500 MPa) as compared to yttria-doped zirconia (Y-TZP) with high strength (800–1500 MPa) but low toughness (~6 MPa $m^{1/2}$). The moderate strength of Ce-TZP ceramics is due to large grains and a high propensity to stress induced phase transformation, which can be autocatalytic [6–8] and may occur at low stresses.

During the past two decades, a new generation of zirconia Ce-TZP based composites was developed with different stabilizers and compositions to obtain tough and strong materials, through microstructure refinement. A Ce-TZP/Al_2O_3 nanocomposite [9,10] in which nanometer Al_2O_3 and 10Ce-TZP particles were trapped within submicron 10Ce-TZP and Al_2O_3 grains, respectively, showed high toughness (9.8 MPa $m^{1/2}$) and a strength of 950 MPa, equivalent to that of conventional 3Y-TZP. A Ce-TZP/$MgAl_2O_4$ nanocomposite with inter and intragranular dispersion of nano-scaled magnesia spinel in a Ce-TZP matrix, developed by Apel et al. [11] showed a biaxial flexural strength of more than 900 MPa. Another approach consists of developing "in situ" platelets reinforced composites with Ce-TZP zirconia reinforced with alumina and strontium or lanthanum hexaaluminate [12,13]. High fracture resistance (up to 12 MPa $m^{1/2}$) and attractive strength (~800 MPa) were also reported for these materials [14].

However, comparison between reported properties is difficult, as the characteristics are generally not obtained with the same methods, while it is evident from prior art that the testing method plays a large role on measured mechanical values. High toughness values (>14 MPa $m^{1/2}$) are for example observed when evaluated by the indentation fracture method [15] or with long propagated cracks in double cantilever beam [12] or double torsion [11] methods, while they are generally lower when measured by single-edge-V-notched beam (SEVNB) [9]. This is due to the variation of transformation morphology and the stress distribution around the crack path, as evidenced recently by Nawa in the case of a Ce-TZP/alumina nanocomposite [16]. Different methods are also used for strength measurement. Parallel to the popular flexural in bending tests, biaxial flexural tests are increasingly used, especially for bioceramics [17–19] due to the simple preparation of required samples. Different configurations were used as piston-on-three balls [20], ball-on-ring [21] and ball-on-three balls [22]. Again, direct comparison between strength values derived from different testing methods is not always valid, and this is generally analyzed through Weibull statistics and the consideration of volume under tensile stresses [23]. In the case of transformation-toughened ceramics, the dependence of tetragonal to monoclinic (t–m) transformation to the testing geometry may also account, but has been little investigated.

In this study, the fracture behavior of a 10Ce-TZP/Al_2O_3/La_2AlO_3 composite exhibiting a high propensity to transformation is investigated. The fracture toughness and flexural strength were evaluated with a focus on the influence of the testing configuration on the flexural strength. Uniaxial and biaxial flexural configurations were performed using four-point bending and piston-on-three balls methods respectively, as model tests often used to the certification of bio-ceramics (see ISO 6872 [24], dedicated to ceramic materials in dentistry).

2. Material and methods

A10Ce-TZP/Al_2O_3/La_2AlO_3 composite, processed by a German laboratory (DOCERAM) in the European framework of Longlife project, currently developed as a biomaterial for dental application was tested. It is composed of 80 vol% 10Ce-TZP with 10 mol% ceria, 10 vol% Al_2O_3 and 10 vol% of (La_2AlO_3). Two types of samples were provided: rectangular bars with polished edges (4 mm × 3 mm × 40 mm) for bending tests and disks (diameter of 15 mm and thickness of 1.2 mm) for biaxial flexural tests. Poisson's ratio and elastic modulus were determined by the resonance vibration method. The density was measured by Archimedes method using distilled water, and the hardness with a Vickers indentation. The microstructure of the composite was observed by scanning electron microscopy (SEM), and X-ray diffraction (XRD) analysis was applied to determine the monoclinic zirconia content [25].

Toughness and strength measurement were conducted on a universal hydraulic INSTRON 8500 testing machine at room temperature (~0 °C) and humidity (RH ~0%). The fracture toughness was determined by the single edge V notched beam (SEVNB) method [26]. Rectangular bars were polished with diamond pastes down to 1 μm to observe the crack extension behavior and notched to a relative depth of 0.4, using a diamond blade with a thickness of 0.2 mm. The notches were then sharpened with a fine razor blade and diamond paste of 1 μm. The samples were annealed at 1200 °C for 20 min to eliminate the machining residual stresses and loaded in a 4-point-bending device (10–35 mm) at a cross-head speed of 5 mm/min. The crack growth resistance curve (*R*-curve) was determined using annealed SENVB samples loaded in three-point bending, with a span of 35 mm and a cross-head speed of 0.005 mm/min. The crack growth resistance was determined, from the recorded load–displacement curve, in terms of stress intensity factor, K_R, plotted versus the crack extension, Δa, optically measured.

Strength measurements were conducted by four-point bending (4PB) tests with roller spacings of 35 and 10 mm and biaxial bending tests (piston-on-three balls, POB) according to ISO 6872, dedicated to ceramic materials in dentistry. The only difference with the ISO recommendation was that the surface of the majority of the samples was polished down to 1 μm with a diamond paste, to be able to observe the t–m transformation with an optical microscope in Normarski contrast. In that case, the strength measurements were conducted on polished and annealed samples (1200 °C for 20 min) in order to suppress any t–m transformation and residual stresses that may be present after the preparation steps. Strength tests were performed at a displacement rate of 5 mm/min, using different testing devices to achieve two stress states: uniaxial tension in four-point bending with rectangular bars and roller spacing of 35 and 10 mm, and Biaxial bending, with disks in piston-on-three balls tests (Fig. 1). To investigate the effect of residual stresses on the strength, a set of "as received" machined disks were also tested in the biaxial configuration. The biaxial flexure strength, σ_B was calculated as follows [24]:

$$\sigma_B = \frac{-0.2837P(X - Y)}{t^2} \quad (1)$$

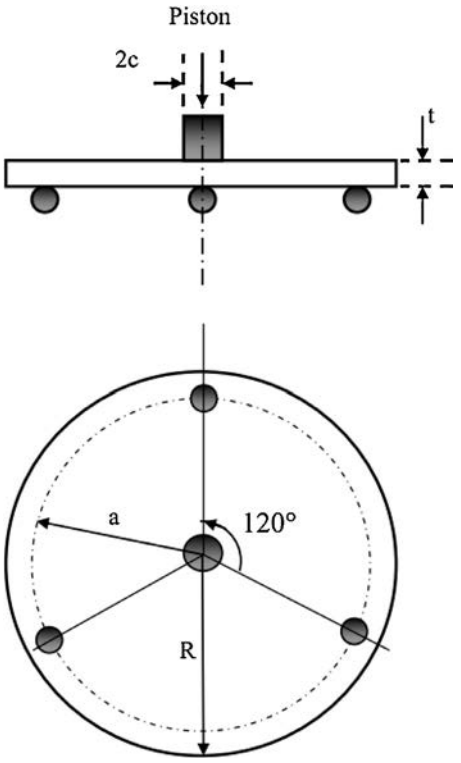

Fig. 1 – Schematic illustration of the piston-on-three balls biaxial flexural test.

where P is the fracture load, t is the specimen thickness, X and Y are respectively given by:

$$X = \ln\left(\frac{c^2}{R^2}\right) + \left(\frac{1-\upsilon}{2}\right)\left(\frac{c^2}{R^2}\right) \quad (2)$$

$$Y = (1+\upsilon)\left[1+\ln\left(\frac{a^2}{R^2}\right)\right] + (1-\upsilon)\left(\frac{a^2}{R^2}\right) \quad (3)$$

where υ is the poison's ratio, $a = 6$ mm is the radius of the supporting circle (Fig. 1), $c = 0.795$ mm is the radius of contact area with the piston and R is the radius of specimen.

The stress field in the disk specimen was analyzed using the finite element (FE) software COMSOL, with Boundary conditions and loading modeled so as to reproduce the conditions of the piston-on-three balls tests: (i) the loading piston is allowed to move only vertically; (ii) the applied load was considered uniformly distributed on the contact area between the piston and the disk; (iii) the support balls positioned at equal distance from each other are fixed in position.

3. Results and discussion

3.1. Microstructure and characteristics

A Scanning electron micrograph of the composite after thermal etching is given in Fig. 2. The three phases are visible with submicron equiaxed zirconia grains (clear grains, with size of 0.6 ± 0.2 μm), micro alumina particles (dark grains with size of 0.3 ± 0.1 μm) located at grain boundaries (and few entrapped

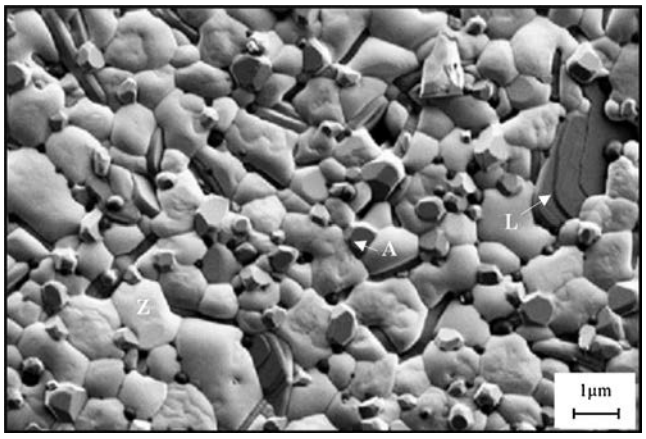

Fig. 2 – SEM micrographs of a polished, thermally etched, sample of the composite showing the three phases: TZP (Z), alumina (A) and lanthanum hexaaluminte (L).

inside zirconia grains), and in situ grown elongated plate-like hexaaluminate grains (length of 1.1 ± 0.4 μm and average aspect ratio of 6). XRD analysis revealed that the composite is entirely retained in the tetragonal phase and no detectable monoclinic zirconia was formed after hydrothermal exposure for 25 h in an autoclave at 134 °C, which indicates an excellent resistance to aging degradation (Fig. 3). The density and the Poisson's ratio of the investigated material are of 5.1618 g/cm^3 and 0.31 respectively. The measured values of hardness and elastic modulus, respectively of 1131 Hv and 245 GPa, are higher than those of conventional 10Ce-TZP ceramics [27].

3.2. Toughness and R-curve behavior

The determined fracture toughness was about 11 ± 0.3 MPa m$^{1/2}$. This is slightly higher than reported values (9.8 MPa m$^{1/2}$) for 10Ce-TZP/Alumina composites where the SEVNB method was used [28]. Fig. 4 shows the crack resistance curve in terms of the stress intensity factor, K_R, plotted versus the crack extension, Δa. Starting from an initial value of 7.2 MPa m$^{1/2}$, K_R increased to a plateau value

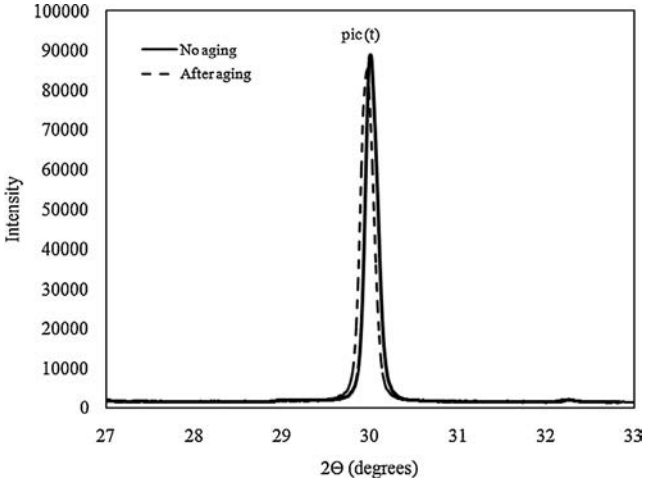

Fig. 3 – XRD patterns before and after aging in an autoclave at 134 °C for 25 h.

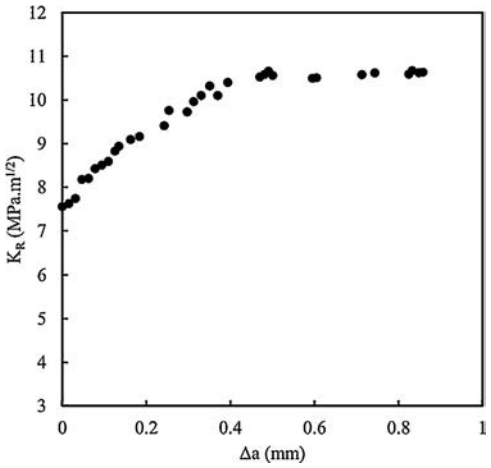

Fig. 4 – Crack growth resistance curve determined on SENVB specimens.

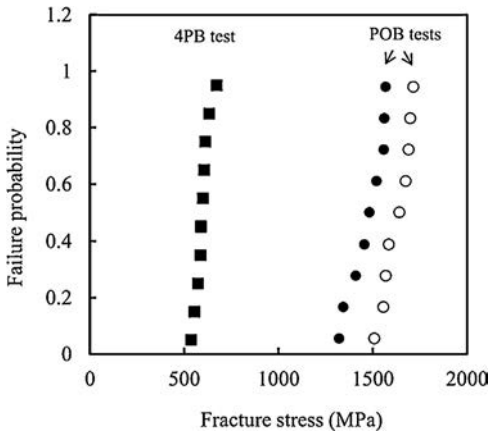

Fig. 6 – Failure probability versus fracture stress for 4-point-bending (4PB) and piston-on-three balls (POB) samples. Open symbols correspond to "as received" POB samples.

of 11 MPa m$^{1/2}$ after a crack extension of 900 μm. This limited *R*-curve effect, as compared to the strong *R*-curve behavior observed in some Ce-TZP based ceramics [27,29,30] is linked to the smaller size of the transformed zone observed and the absence of marked autocatalytic phase transformation for this geometry (Fig. 5). It can be noticed that the measured SEVNB fracture toughness corresponds to the maximum plateau region, corresponding to the long crack regime.

3.3. *Flexural strength*

3.3.1. *Statistical analysis*

The strength data were analysed according to the Weibull distribution [23]:

$$P_i = 1 - \exp\left(-\left(\frac{\sigma_i}{\sigma_m}\right)^m\right) \quad (4)$$

where P_i is the probability of failure under an applied stress σ_i, m is the Weibull modulus, and σ_m is a characteristic strength, corresponding to 63% of probability of failure.

Fig. 6 shows the strength distribution of the two flexural configurations. The determined average strengths and Weibull modulus are given in Table 1. The Weibull modulus was the same for the polished and annealed samples, tested in both configurations, which is consistent with identical flaw population in these samples. The biaxial strength decreased after polishing and annealing, which may be attributed to the suppression of the compressive residual stresses due to induced

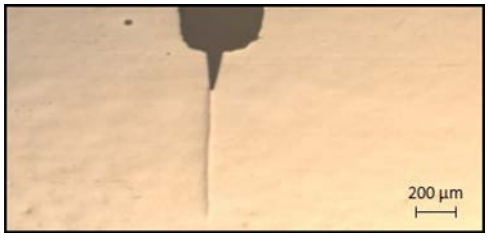

Fig. 5 – Optical micrograph of the transformation zone in a fractured SEVNB sample.

Table 1 – Strength, σ_R, and Weibull modulus, m, obtained with 4-point-bending (4PB) and piston-on-three balls (POB) tests.

Test method	Surface condition	σ_R (MPa)	m
4PB	Polished and annealed	596 ± 38	18
POB	Polished and annealed	1470 ± 94	18
POB	As received	1626 ± 73	25

phase transformation during machining, as it was already observed for Ce-TZP/Al_2O_3 nanocomposites [10,31]. The most striking result is that 4-point-bending strength was about 2.5 times lower than the biaxial one. Such a large difference is in line with results published separately on the same material, a 10Ce-TZP/30 vol% Al_2O_3 nanocomposite, for which the biaxial strengths measured by the piston-on-three balls and 4-point bending methods were reported to be 1422 MPa [32] and 740 MPa [9] respectively. These differences were not documented, since each paper had a separate objective.

For ceramic materials, the effect of the loading configuration on the fracture strength is generally well described by the Weibull analysis [18]. This is achieved by introducing the effective volume or the effective surface, for volume or surface defects respectively [33]. By applying this analysis, the predicted ratio between the fracture strengths, σ_{4PB} and σ_{POB}, corresponding respectively to the 4PB and POB tests used in the present work, was calculated as follows:

$$\left(\frac{\sigma_{4PB}}{\sigma_{POB}}\right) = \left(\frac{S_{POB}}{S_{4PB}}\right)^{1/m} \quad (5)$$

where S_{4PB} and S_{POB} are the effective surfaces determined according to [18], respectively for the uniaxial 4PB and the biaxial POB flexural tests. With calculated values of 47.6 mm^2 and 11.9 mm^2 for S_{4PB} and S_{POB} respectively, the biaxial flexural strength σ_{POB}, predicted from the uniaxial measurement was of 644 MPa. This corresponds only to an increase of 8% and cannot explain the high value of the measured biaxial flexural strength.

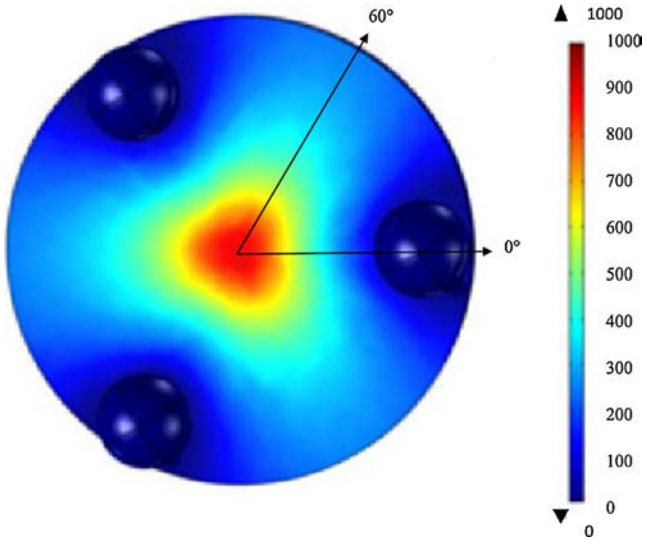

Fig. 7 – First principal stress field on the tensile surface for the biaxial (POB) test.

3.3.2. *Finite element analysis of the stress field*

The FE modeling allowed to determine the stress distribution and the maximum principal stresses for the biaxial test. The stress distribution on the tensile side of the sample for the applied load at failure, shown in (Fig. 7), is triply axisymmetric, due to the three supporting balls. A tensile stress concentration is located at the center of the disk, corresponding to the position of the loading piston (red area) and the support areas are subjected to compressive stresses (dark blue areas). In contrast with the typical constant stress (between the two loading points) for the 4PB configuration, the principal stresses show a fast decay radially toward the disk periphery, as shown along the 60°-directions of the tensile plane in Fig. 8. Such profile is typical of biaxial bending configurations with stress concentration as also reported by Börger et al. for the ball on three balls test [34].

3.3.3. *Transformation behavior*

The transformation behavior was investigated considering the load–displacement curves (Fig. 9) and the evolution of the transformed zones on the tensile surfaces of both 4PB and POB

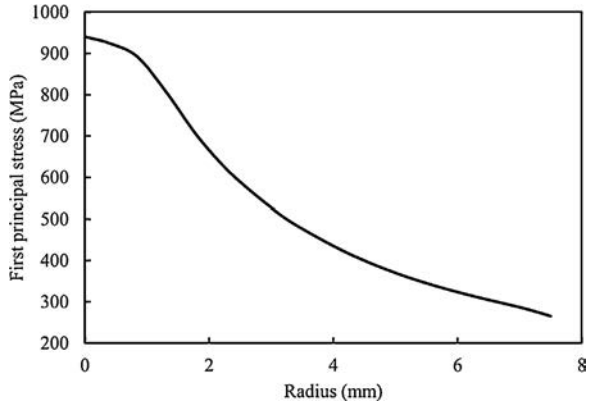

Fig. 8 – First principal stress versus distance to the center, along the 60° direction of the tensile plane, for the POB test.

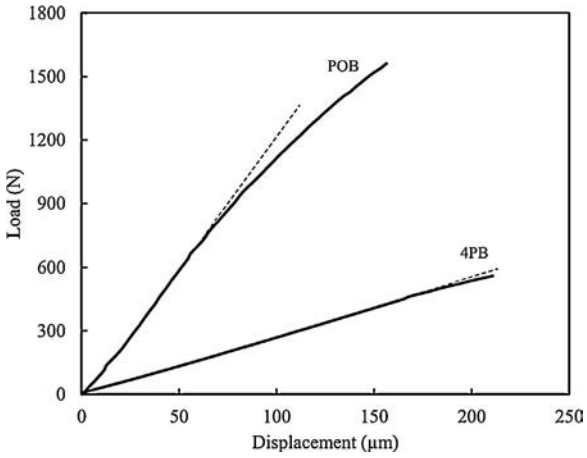

Fig. 9 – Load versus displacement curves in four-point bending (4PB) and biaxial bending (POB) tests.

samples. For that, some samples were unloaded during the flexural tests for optical examinations with Normaski interference contrast, then reloaded. The procedure was repeated at different loading levels until failure. As shown in Fig. 9, the loading curves for four-point bending samples were linear until a stress level corresponding to 90% of the fracture strength, where a low nonlinearity appeared. In contrast, the biaxial bending disks showed a nonlinear behavior starting well before failure at a stress level less than 40% of the fracture strength for this configuration.

The evolution of the transformation zones, shown in Figs. 10 and 11 respectively for 4PB and POB samples shows the autocatalytic nature of the tetragonal to monoclinic phase transformation in the studied composite and that transformation occurs before failure for both loading configurations. However the transformation zones are different. In the biaxial POB configuration (Fig. 11) transformed bands located at the center of the sample, where the stress is maximum, appeared at a low applied stress level (<500 MPa). When the load was increased, the bands multiplied and propagated radially. From a load of 935 MPa, a circular transformation zone appeared at the center of the disk and expanded with a large number of individual branches as the stress increased. For the rectangular 4PB specimens (Fig. 10), irregularly spaced transformation bands with about 30 μm width were observed just before failure (around 90% of the failure stress). For both configurations, the fracture was initiated along transformation bands normal to the maximum principal stress direction. To characterize the transformation rate, the relative transformed area within a circle equivalent to the effective surface for the POB disk (white circle in Fig. 12) was estimated at the failure stress, and was of 80%. In comparison, this ratio is less than 1% for 4PB bars. Taking into account to strength sensitivity to the compressive residual stresses resulting from the phase transformation, the large transformed zone observed in the biaxial POB tests could contribute to the high value measured for this configuration.

The load–displacement behavior and the evolution of the transformation zones confirm the two transformation stages reported by Rauchs et al. [35] for 9Ce-TZP zirconia materials investigated under different loading

Fig. 10 – Transformation zones observed at different applied loads on the tensile surface of a 4-point-bending sample.

configurations: a homogeneous phase transformation, accompanied by increasing transformation strain with the applied stress, and an autocatalytic phase transformation with the formation of transformation bands normal to the maximum principal stress. The critical stresses at the onset of the homogeneous phase transformation, σ_H, correspond to the initial deviation from linearity of the loading curves. The critical value for the autocatalytic phase transformation, σ_A, was

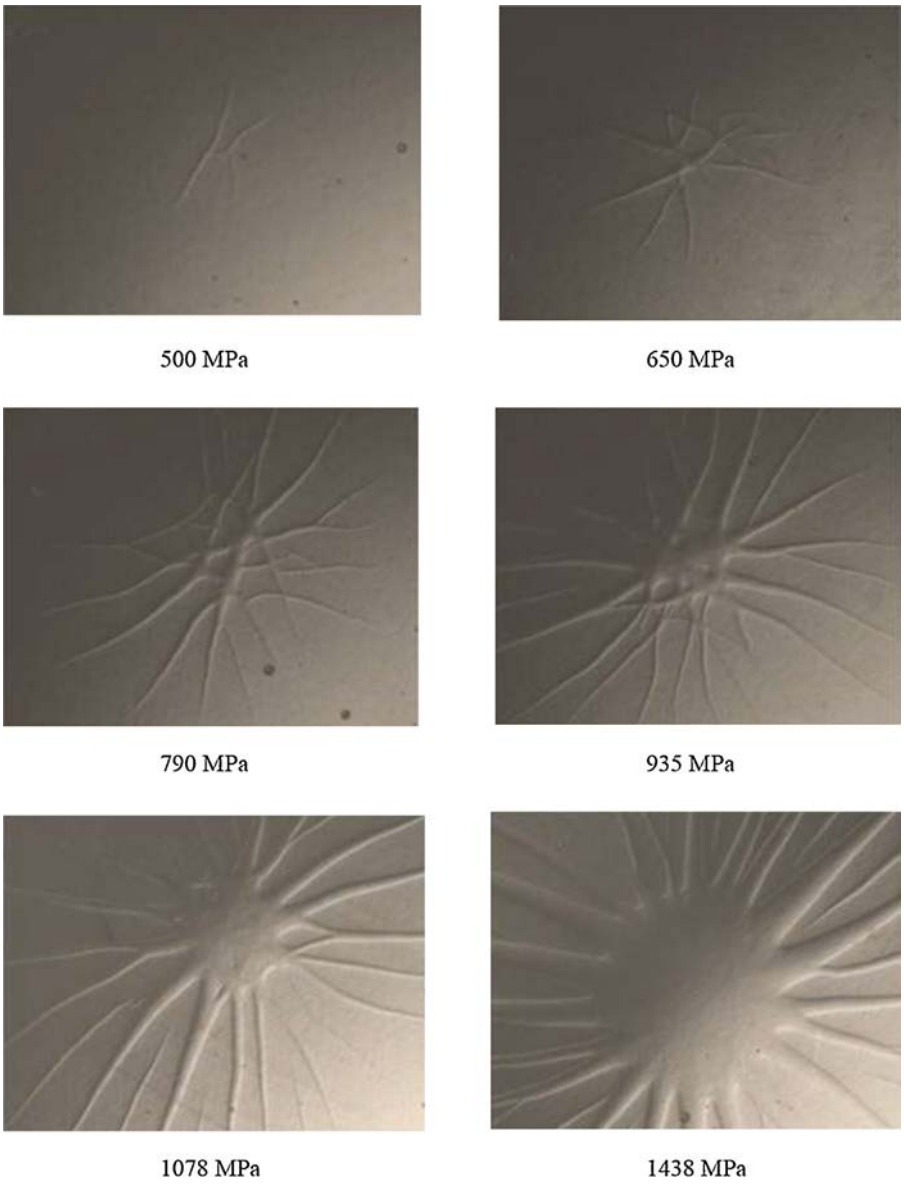

Fig. 11 – Transformation zones observed at different applied loads on the tensile surface of a POB disk.

Fig. 12 – Illustration of the transformation zone at failure. The circle corresponds to the effective surface for the POB configuration.

calculated at the first apparition of the transformed bands for POB disks. For 4PB bars, it was deduced from the linear stress distribution on the tensile surface, outside the supporting points. σ_A was taken as the stress value corresponding to position of the outer most transformed bands. The experimentally determined values are given in Table 2 for the two testing configurations. The critical stresses, σ_H, and σ_A, are equivalent (within the confidence interval) for the uniaxial 4PB test,

Table 2 – Critical transformation stresses in four-point bending (4PB) and piston-on-three balls (POB) tests.

σ_H (MPa)		σ_A (MPa)	
4PB	POB	4PB	POB
548	870	538	<486

whereas a great difference is observed between the values of the biaxial POB test. This difference is more important than that observed by Rauchs et al. [35] when four-point bending and ring-on-ring tests were compared. It is to note that for the last configuration, the transformation zone was not continuous as in the current work, but the transformation bands were randomly oriented in a netlike structure.

In order to determine a criterion for the tetragonal-to-monoclinic phase transformation, equivalent stresses have been calculated from the critical stresses of the homogeneous and the autocatalytic phase transformations for the two investigated loading configurations. The results are represented in two types of transformation diagrams [35]: a transformation diagrams with shear-dilatant criterion in which the hydrostatic stress, σ_h, is plotted versus the Von Mises stress, σ_v, and a multiaxial transformation diagrams based on the maximum principal stresses, σ_1, and σ_2, obtained from the FE calculations. The diagrams corresponding to the homogeneous and

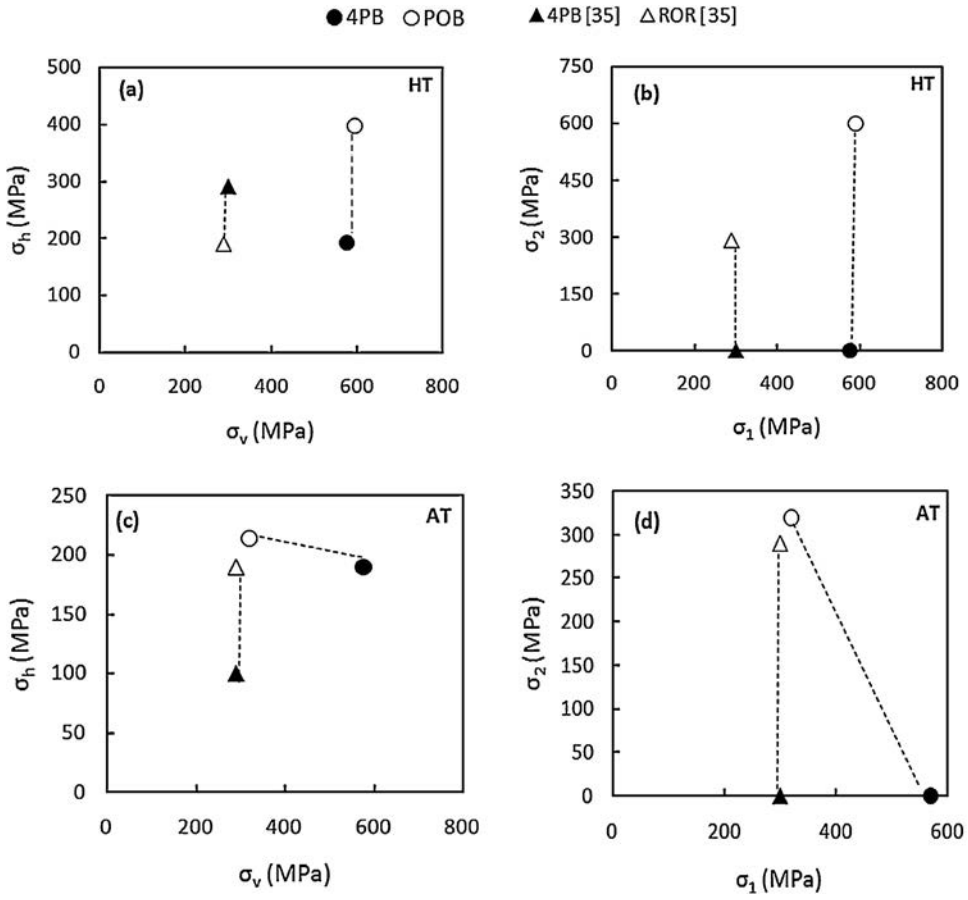

Fig. 13 – σ_h–σ_v diagrams with shear-dilatant criterion (a and c) and multi-axial transformation diagrams (b and d) for homogeneous (HT) and autocatalytic (AT) transformations. Comparison of the results of the 4PB and POB tests, corresponding respectively to solid and open circle symbols, with those of Ref. [35].

the autocatalytic transformations are shown in Fig. 13, where the results of Rauchs et al. [35] are also reported for comparison. They concern a 9Ce-TZP ceramic with grain size of 2.5 μm, loaded in 4PB and ring-on-ring configurations, for which the onset of both transformations could be predicted with the maximum principal stress criterion. For the 4PB and POB configurations used in this study, the homogeneous phase transformation occurs in the composite at equivalent stresses when the Von Mises stress (Fig. 13a) or the maximum principal stress (Fig. 13b) are considered. This means that both criteria could be applied for the homogeneous transformation. However, neither criteria could be applied to the onset of the autocatalytic transformation, as in the two transformation diagrams, it occurs at different equivalent stresses for 4PB and POB configurations. Both the maximal principal stress and the hydrostatic stress have significantly lower values for POB samples. It can thus be concluded that the high strength value obtained for the biaxial POB tests, can be attributed to the singular autocatalytic transformation behavior in this configuration, which induces high compressive stresses at the tensile surface of the samples at early stage of loading.

These results are of importance, since piston-on-three balls tests are very often used to qualify bioceramics, especially for dental applications, while it could overestimate strength data because of a peculiar stress field. Also, it is clear that the comparison of strength data in such highly transformable zirconia based ceramics and composites must not be compared if not conducted with the same tests. These results also question about of the most relevant test for a given ceramic product, if it has to be processed by a transformable ceramic. It may be argued, for example in the case of a dental implant, that pure uniaxial bending is the most likely to represent the stress state during use. On the other side, the fact that the stresses are localized at the tip of the threats and then decrease rapidly with distance to the threat tip are in favor of considering a stress field as in piston-on-three balls. As these composites are currently developing fast and are considered as potential materials for dental implants, it is urgent to define the most relevant tests and to understand/describe better the criteria applicable for the autocatalytic transformation, in order to apply correct mechanical behavior laws to the design of these structures.

4. Conclusion

Strength measurements conducted in uniaxial and biaxial flexural configurations using 4-point-bending and piston-on-three balls methods give very different results for highly transformable zirconia-based composites. The mean strength obtained for the uniaxial tests was of 596 MPa and that of the biaxial tests was of 1470 MPa. The large difference between these values could not be predicted by the statistical Weibull analysis, as it is generally the case for ceramic materials and are attributed to different autocatalytic transformation behaviors under the two testing configurations.

The results emphasize that a direct comparison between reported strength values for zirconia based composites is not always valid. The relevance of a given strength qualification method to a given product should be checked before the use as an implant material.

Acknowledgements

Funding for this collaboration between the two groups was provided by a grant from the Rhône–Alpes Region (CMIRA framework). Doceram Medical is acknowledged for processing the composites used during this work, in the framework of the LONGLIFE European project (www.longlife-project.eu). LONGLIFE received funding from the European Community's Seventh Framework Program (FP7/2007-2013) under grant agreement no 280741.

REFERENCES

[1] Marshall D, Evans A, Drory M. Transformation toughening in ceramics. Fract Mech Ceram 1983;87:461–87.
[2] Green D, Hannink R, Swain M. Transformation toughening of ceramics. Boca Raton, FL: CRC Press; 1988.
[3] Evans AG. Perspective on the development of high-toughness ceramics. J Am Ceram Soc 1990;73(2):187–206.
[4] Hannink RHJ, Kelly PM, Muddle BC. Transformation toughening in zirconia-containing ceramics. J Am Ceram Soc 2000;83:461–87.
[5] Swain MV, Rose LRF. Strength limitations of transformation-toughened zirconia alloys. J Am Ceram Soc 1986;69(7):511–8.
[6] Reyes-Morel P, Chen IW. Transformation plasticity of CeO_2-stabilized tetragonal zirconia polycrystals. I. Stress assistance and autocatalysis. J Am Ceram Soc 1988;71(5):343–53.
[7] Chien FR, Ubic FJ, Prakash V, Heuer AH. Stress-induced martensitic transformation and ferroelastic deformation adjacent microhardness indents intetragonal zirconia single crystals. Acta Mater 1998;46:2151–71.
[8] Sun QP, Li XJ, Li Z. Autocatalytic transformation, materials softening and toughening of single and multi-phase CE-TZP ceramics. Adv Fract Res 1997;2:1089–96.
[9] Nawa M, Bamba N, Sekino T, Niihara K. Tough and strong Ce-TZP/alumina nanocomposites doped with titania. Ceram Int 1998;24(7):497–506.
[10] Benzaid R, Chevalier J, Saâdaoui M, Fantozzi G, Nawa M, Diaz LA. Slow-crack propagation behavior in Ce-TZP/Al_2O_3 nanocomposites. Biomaterials 2008;29:1560–5.
[11] Apel E, Ritzberger C, Courtois N, Reveron H, Chevalier J, Schweiger M, et al. Introduction to a tough, strong and stable Ce-TZP/$MgAl_2O_4$ composite for biomedical applications. J Eur Ceram Soc 2012;32(11):2697–703.
[12] Cutler RA, Mayhew RJ, Prettyman KM, Virkar AV. High-toughness Ce-TZP/Al_2O_3 ceramics with improved hardness and strength. J Am Ceram Soc 1991;74(1):179–86.
[13] Miura M, Hongoh H, Yogo T, Hirano S, Fujll T. Formation of plate-like lanthanum-β-aluminate crystal in Ce-TZP matrix. J Mater Sci 1994;29(1):262–8.
[14] Kern F. A comparison of microstructure and mechanical properties of 12Ce-TZP reinforced with alumina and in situ formed strontium- or lanthanum hexaaluminate precipitates. J Eur Ceram Soc 2014;34(2):413–23.
[15] Tanaka K, Tamura J, Kawanabe K, Nawa M, Uchida M, Kokubo T, et al. Ce-TZP/Al_2O_3 nanocomposites as a bearing material in total joint replacement. J Biomed Mater Res 2002;63:262–70.

[16] Nawa M, Yamada K, Kurizoe N. Effect of the t–m transformation morphology and stress distribution around the crack path on the measured toughness of zirconia ceramics: a case study on Ce-TZP/alumina nanocomposite. J Eur Ceram Soc 2013;33(3):521–9.
[17] Chung SM, Yap AUJ, Chandra SP, Lim CT. Flexural strength of dental composite restoratives: comparison of biaxial and three-point bending test. J Biomed Mater Res Part B Appl Biomater 2004;71(2):278–83.
[18] Jin J, Takahashi H, Iwasaki N. Effect of test method on flexural strength of recent dental ceramics. Dent Mater J 2004;23:490–6.
[19] Kelly RD, Fleming GJP, Hooi P, Palin WM, Addison O. Biaxial flexure strength determination of endodontically accessed ceramic restorations. Dent Mater 2014;30(8):902–9.
[20] Kirstein AF, Woolley RM. Symmetrical bending of thin circular elastic plates of equally spaced point supports. J Res Natl Bur Stand 1967;71:1–10.
[21] McKinney KR, Herbert CM. Effect of surface finish on structural ceramic failure. J Am Ceram Soc 1970;53:513–6.
[22] Godfrey DJ, John S. Disc flexure tests for the evaluation of ceramic strength: ceramic materials and components for engines. Proc Second Int Symp 1986;14(7):657–65.
[23] Weibull W. A statistical distribution function of wide applicability. J Appl Mech 1951;18:293–305.
[24] ISO 6872. Dentistry – ceramic materials. Geneva: International Organization for Standardization; 2008.
[25] Toraya H, Yoshimura M, Somiya S. Calibration curve for quantitative analysis of the monoclinic-tetragonal ZrO_2 system by X-ray diffraction. Commun Am Ceram Soc 1984:119–21.
[26] Kübler J. Fracture toughness of ceramics using the sevnb method: first results of a joint VAMAS/ESIS round robin. Ceramic Engineering & Science Proceedings. J Am Ceram Soc 1999;20:494–502.
[27] El Attaoui H, Saâdaoui M, Chevalier J, Fantozzi G. Static and cyclic crack propagation in Ce-TZP ceramics with different amounts of transformation toughening. J Eur Ceram Soc 2007;27(2–3):483–6.
[28] Nawa M, Kurizoe N, Okamoto Y, Ueno A. Transformation-induced plastic deformation in Ce-TZP/alumina nanocomposite generated during fatigue tests at room temperature. J Eur Ceram Soc 2014;34(16):4337–45.
[29] Liu T, Mai YW, Swain MV, Grathwohl G. Effects of grain size and specimen geometry on the transformation and R-curve behaviour of 9Ce-TZP ceramics. J Mater Sci 1994;29(3):835–43.
[30] Rauchs G, Fett T, Munz D. R-curve behaviour of 9Ce-TZP zirconia ceramics. Eng Fract Mech 2002;69(3):389–401.
[31] Marro FG, Mestra A, Anglada M. Contact damage in a Ce-TZP/Al_2O_3 nanocomposite. J Eur Ceram Soc 2011;31(13):2189–97.
[32] Ban S, Hideo S, Yasuhiko S, Hideo N, Nawa M. Biaxial flexure strength and low temperature degradation of Ce-TZP/Al_2O_3 nanocomposite and Y-TZP as dental restoratives. J Biomed Mater Res Part B Appl Biomater 2008;87B(2):492–8.
[33] Shetty DK, Rosenfield AR, Duckworth WH, Held PR. A biaxial-flexure test for evaluating ceramic strengths. J Am Ceram Soc 1983;66(1):36–42.
[34] Börger A, Supancic P, Danzer R. The ball on three balls test for strength testing of brittle discs: stress distribution in the disc. J Eur Ceram Soc 2002;22:1425–36.
[35] Rauchs G, Fett T, Munz D, Oberacker R. Tetragonal-to-monoclinic phase transformation in CeO_2-stabilised zirconia under multiaxial loading. J Eur Ceram Soc 2002;22:841–9.